Earth and Planetary Science Letters 544 (2020) 116363

Contents lists available at ScienceDirect

Earth and Planetary Science Letters

www.elsevier.com/locate/epsl

Reversing transverse dunes: Modelling of airflow switching using 3D computational fluid dynamics

Derek W.T. Jackson [a,b,*], Andrew Cooper [a,b], Andrew Green [b], Meiring Beyers [c], Emilia Guisado-Pintado [d,a], Errol Wiles [e], Keegan Benallack [b], Matt Balme [f]

[a] Centre for Coastal & Marine Research, School of Geography & Environmental Sciences, Ulster University, Northern Ireland, United Kingdom
[b] Geological Sciences, University of KwaZulu-Natal, South Africa
[c] Klimaat Consulting & Innovation Inc., Guelph, Canada
[d] Department of Physical Geography and Regional Geographic Analysis, University of Seville, Seville, Spain
[e] South African Institute for Aquatic Biodiversity, Somerset Street, Grahamstown, South Africa
[f] School of Physical Sciences, The Open University, Walton Hall, Milton Keynes, United Kingdom

ARTICLE INFO

Article history:
Received 13 December 2019
Received in revised form 15 May 2020
Accepted 25 May 2020
Available online 9 June 2020
Editor: J.-P. Avouac

Keywords:
aeolian
reversing dunes
computational fluid dynamics
airflow
transverse ridges

ABSTRACT

Airflow dynamics across dune surfaces are the primary agent of sediment transport and resulting dune migration movements. Using 3D computational fluid dynamic modelling, this study examined the behaviour of near surface airflow travelling over transverse (reversing) dunes on a beach system. Wind direction was modelled in two opposing directions (both perpendicular to dune crestline) to investigate surface alteration of flow on the dune topography. Surface shear stress, velocity streamlines and potential sediment flux were extracted from the modelling. The work shows that under SW winds the surface (under the configuration measured) underwent almost 10% more aeolian flux than with opposing NE winds of the same magnitude. Differences were also noted in the airflow behaviour with SW winds staying attached to the surface with less turbulence while NE winds had detached flow at dune crests with more localised turbulence. The work provides detailed insights into how 3D airflow behaviour is modified according to incident flow direction of reversing dune ridges and the resulting implications for their topographic modification. These dune types also provide interesting analogues for similarly scaled Transverse Aeolian Ridges found on Mars and the findings here provide important understanding of flow behaviour of such landforms and their potential movement.

1. Introduction

Airflow over terrestrial sand dunes is the fundamental forcing mechanism in dune landform dynamics. If sufficiently strong, wind will transport sediment and move aeolian landforms in the dominate direction of the local wind regime. Depending on the availability of sediment, the directionality and intensity of local winds, a variety of dune types and dynamics unfold (Courrech du Pont et al., 2014; Gao et al., 2015; McKee, 1979). Acceleration of airflow over dune crests/brink is a key parameter in driving dune migration and slip face dynamics and an understanding of localised interaction of the dune landform with wind forcing is central in unravelling larger dune field-scale behaviour and dynamics.

Unvegetated (arid/semi-arid climates) dune fields provide excellent opportunities to examine airflow dynamics over various types and scales of dune landforms and to explore how they are forced by wind action. The three dimensional surface over which a lower boundary layer abuts, helps adjust surface airflow and consequently aeolian transport on dunes. The use of Computational Fluid Dynamic (CFD) modelling in recent years enables investigation of the 3D behaviour of airflow over complex terrain (Paterson and Holmes, 1993), helping to provide new insights into heterogeneous surface flow and aeolian transport on dune surfaces on a large (dunefield) scale. Recent developments in this modelling applied to dunes (e.g. Anderson and Chamecki, 2014; Bristow et al., 2019; Jackson et al., 2011, 2013a,b, 2015; Smith et al., 2017a,b; Smyth, 2016; Smyth et al., 2011, 2012, 2013, 2014) has helped shed new light on the complex patterns of airflow-aeolian transport-dune dynamics. Field validation of a CFD modelling approach (Jackson et al., 2011) shows good agreement with *in situ* 3D measurements of wind flow and CFD proves to be an effective tool in examining wind flow over small (dune length) scales (Jackson et al., 2013b, 2015; Smith et al., 2017b) and even at larger dune field scales (Jackson et al., 2013b, 2015; Smith et al., 2017b).

* Corresponding author.
E-mail address: d.jackson@ulster.ac.uk (D.W.T. Jackson).

https://doi.org/10.1016/j.epsl.2020.116363

Building reliability and capability in CFD modelling has opportunities for understanding aeolian processes in places where field work is almost impossible. On Mars, for example, aeolian bedforms with length-scales ranging from centimetres to kilometres are common, and are obviously unvegetated (Greeley and Iversen, 1985; Silvestro et al., 2013; Sullivan et al., 2005). Some martian bedforms are actively migrating (Bourke et al., 2008; Chojnacki et al., 2011; Silvestro et al., 2010; Sullivan et al., 2008), but many others show no signs of movement, and why this should be the case is not well understood. The availability of very high resolution data (25 cm/pixel images and 1 m/pixel terrain models) from the HiRISE camera (McEwen et al., 2007), as well as the existence of several mature global (Haberle et al., 1993; Lewis et al., 1999) and mesoscale atmospheric models (Spiga and Forget, 2009; Toigo and Richardson, 2002), means that CFD can be applied directly to martian bedforms as a proxy for *in situ* wind field measurements, to answer these questions about how martian bedforms migrate and when they can become active.

Reversing dunes (Bristow et al., 2010; Burkinshaw et al., 1993; Lindsay, 1973) are one of the nine types of dunes identified by McKee (1979) and are effectively transverse or barchan dunes whose profiles dramatically alternate from one face of the dune to the other over time (Bagnold, 1941; Cornish, 1897; Dann, 1939; King, 1918). The reversing nature and the 180-degree change in slip face orientation gives them their title (Lindsay, 1973; McKee, 1979). Reversing transverse dunes occur when subjected to a reversing wind regime (Selby et al., 1974) and so are relatively rare aeolian landforms. They can occupy 'stable' dunefield dynamics where there are sometimes low net migration rates taking place. This can result in dunes effectively being 'locked' within a defined spatial area under strong (largely equal) bi-directional wind regimes. Unvegetated dunes of the size and type described here are free to respond rapidly to the direct forcing of winds moving across their surfaces and will respond topographically to changes in wind direction in timescales of just several hours to days. How and why they move under bi-directional winds dictates the net dynamics of the dunefield.

It is still not fully understood how surface airflow becomes modified when at the onset of flow reversal over transverse dunes and when stoss (windward) slopes adopt the role of lee (downwind shadow) slopes and *vice versa* at the onset of this reversal. In this paper, a detailed 3D surface topography derived from ground-based terrestrial laser scans of transverse (reversing) dunes at Mpekweni beach, South Africa are used as a surface to run 3D computational fluid dynamic modelling of airflow in two opposing (and orthogonal to the dune crests) directions (SW and NE) in order to examine the airflow behaviour under each scenario.

1.1. Location

Mpekweni is located ~80 km south of East London, South Africa. The main dunefield stretches 3 km along the coast and is positioned between two estuaries, Mpekweni in the west and Mtati in the east (Fig. 1a, b). The dune field is composed of sediment with D_{50mean} of 0.28 mm and is actively mobile between the fixed Pleistocene (70 m high) fossil dunes and the beach. The bedforms shown in Fig. 1b have crest-to-crest wavelengths of around 60 m and have heights of approximately 5 m (Fig. 2) as shown in an extracted profile A-B in Fig. 1b. The area is subjected to strong bi-modal winds with the more frequent winds from the west but at times more intensive winds from the east (see insert, Fig. 1a). Localised steering of winds appears to push airflow into a more shore parallel direction at the beach, along shore in both directions.

Along the eastern South African coastline, persistent and strong coast-parallel winds create obvious alongshore aeolian drift that is manifest in the development of large unvegetated transverse dunes (Tinley, 1985). The largest known mobile coastal dunefields in the east South Africa are the 60 km long, 2 km wide Alexandria coastal dune field (Illenberg and Rust, 1988), and the 35 km long, 1 km wide example at Jeffrey's Bay (Tinley, 1985). However, between Port Alfred and East London (200 km) there are semi-continuous stretches of wide, dry, sandy beach on which have developed persistent mobile aeolian dunes oriented normal to the shoreline. These dunes abut densely vegetated coastal dunes and migrate under strong alongshore winds (see Burkinshaw et al., 1993; Burkinshaw and Rust, 1993). Long-term geological evidence, in the form of lag accumulations in the troughs of these features, suggests reversals in migration due to local alongshore steering and reversals of winds (Cooper et al., 2013). Burkinshaw and Rust (1993) showed that these reversals were in response to changes between summer and winter wind regimes. Studies from the neighbouring Alexandria dune field indicate a net northeasterly flux in the dunes of between 15 to 30 $m^3\ yr^{-1}$ (Burkinshaw and Rust, 1993)

2. Materials and methods

Acquisition of accurate and detailed topographic data is crucial in providing 3D airflow modelling with a realistic underlying surface with which to interact. Here we gathered topographic data of the dunes at a high-resolution and incorporated this into modelling of the airflow.

2.1. Surface topography

A detailed topographic surface was generated using a high-resolution terrestrial laser scanner (Faro X330) and re-gridded to a surface resolution of 0.1 m × 0.1 m grid cell size. All laser scan positions and target spheres were geo-located using a DGPS system with an accuracy of +/- 0.01 m. A total area of interest measuring 750 m × 750 m (Fig. 3) was examined using 28 TLS scan setups to minimise survey shadow (gaps) over the terrain.

2.2. CFD airflow modelling

A computational wind simulation was performed using the open-source computational fluid dynamic (CFD) suite OpenFOAM which has been used and successfully validated in a number of other dune environments (Cornwall et al., 2018; Jackson et al., 2011, 2013a, 2015; Smith et al., 2017a,b; Smyth et al., 2012, 2013, 2014). The extent of the computational domain encompassing the dune field site was 400 m by 400 m by 100 m in the vertical with local mesh refinement near the dune surface. The dune terrain geometry was pre-processed and re-meshed from the high-resolution scan into a stereolithographic mesh file using in-house python code that employs a Delaunay triangulation of the scanned mesh points.

The horizontal and vertical mesh size near the surface of the computational terrain was approximately 1.5 m and 0.4 m, respectively. During the first round of simulations, no mesh refinement, or mesh convergence tests were conducted as the purpose was to gain initial insights into the general wind flow behaviour across the dune field under switching wind conditions.

The CFD model employed a steady state incompressible solver (simpleFOAM) with a Re-Normalisation Group (RNG) k-ε turbulence model. The inlet atmospheric boundary layer (ABL) profile for the horizontal wind velocity, turbulent kinetic energy and dissipation rate, was applied in accordance with Richards and Hoxey (1993) i.e.:

$$\frac{u}{u_*} = \frac{1}{\kappa} ln\left(\frac{(z + z_0)}{z_0}\right) \quad (1)$$

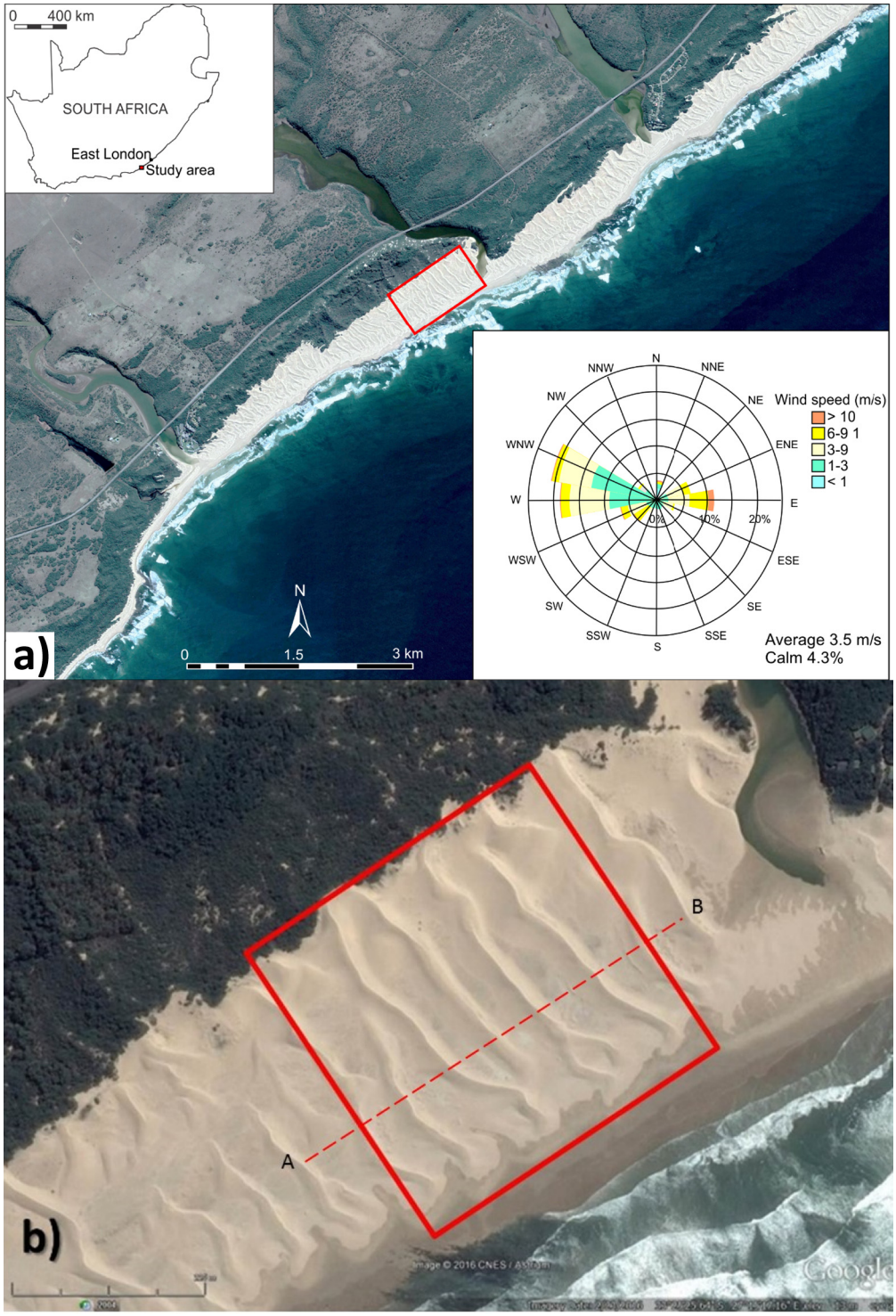

Fig. 1. (a) Mpekweni site in South Africa and the wind rose of Port Alfred (40 km SW) (b) the northern section of the dune field surveyed. Dashed line A-B indicates the cross-section extracted from the surface of the dunes. Note: Lighting is from the left. Image Source: Google Earth. (For interpretation of the colours in the figure(s), the reader is referred to the web version of this article.)

$$k = \frac{u_*^2}{\sqrt{C_\mu}} \tag{2}$$

$$\varepsilon = \frac{u_*^3}{\kappa z} \tag{3}$$

where u is the horizontal ABL wind velocity at height z, u_* the ABL shear velocity, κ the von Karman constant and C_μ is a modelling constant of the k-ε turbulence model (0.09). Terrain surface roughness was set at $z_0 = 0.05$ m. The inlet profile was set up with reference wind speed of 10 ms^{-1} at reference height of 10 m above the terrain, and an aerodynamic surface roughness of 0.05 m. The modelling approach was found to provide a good approximation of dune wind flow characteristics (compared to in situ measurements of airflow), especially for representing dune wake zone recirculation (Jackson et al., 2013a, 2011; Smyth, 2016; Smyth et al., 2014, 2013).

Although no direct wind measurements were sampled directly in the field as the main thrust of the study was to investigate

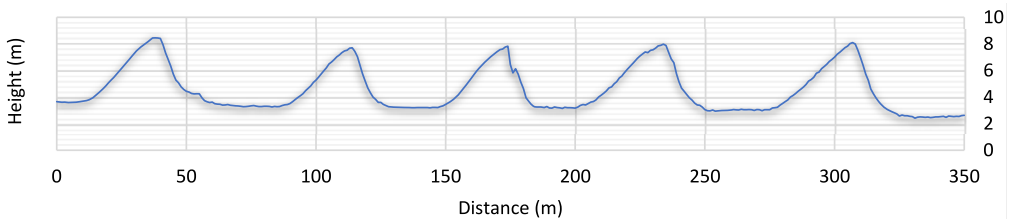

Fig. 2. Cross-sectional profile A-B as annotated in Fig. 1b showing 5 m high transverse dunes with around 60 m wave lengths.

the onset of reversal (rare to isolate in field conditions), two wind direction scenarios were simulated, with choices based on the orthogonal directions to dune crest orientation giving incident wind approaches from the SW (winds originating from the SW) and from the NE (Fig. 1a inset). An offset is noted between these directions and those from the closest meteorological station at Port Alfred 40 km away to the SW that shows a predominant W and E directionality in regional winds. This offset is likely due to localised flow steering (Jackson et al., 2013b) from the 70-80 m high coastal topography in the form of high, fossilised Pleistocene dunes running along the entire back beach of the site which redirect (steer) winds at the beach to the SW when regional winds are from the West.

The CFD results are presented in the form of surface flow streamlines and superimposed over 3-D topographic data to illustrate a few key wind flow observations. Additionally, the terrain surface shear velocity distribution is also shown to highlight the difference in the dune bed shear stress under the two opposing flow scenarios along with corresponding aeolian flux predictions (below).

2.3. Calculation of aeolian flux

The near surface shear stress and shear velocity fields obtained from the CFD simulation results were used to derive a localised sediment flux across the dunefield. The sediment flux equation employed here (defined as Q_{flux} in our figures) follows the approach as outlined in Smith et al. (2017a) to determine a slope-corrected total transport flux, namely,

$$q = Gq_{sat} \tag{4}$$

$$q_{sat} = 2\alpha_1 \frac{\rho}{g}(u_*^2 + u_{*t}^2) \times \left(u_* \frac{2}{K}\sqrt{\frac{z_1}{z_m} + \left(1 - \frac{z_1}{z_m}\right)\frac{u_{*t}^2}{u_*^2}} - \frac{2u_{*t}}{K} + u_{st}\right)$$

$$u_{*t} = A\sqrt{\frac{\sigma - \rho}{\rho} gd}$$

$$z_m = \frac{u_*^2}{g}$$

$$u_{st} = \frac{u_{*t}}{K} ln \frac{z_1}{k_0} - \sqrt{\frac{2gd\sigma}{3\alpha_1 C_d \rho}}$$

$$G = \frac{tan(\alpha)}{cos(\theta)(tan(\alpha) + tan(\theta))}$$

where α_1 (0.35) and z_1 (0.005) are model constants, α is the repose angle of dry sand (34°), θ is the slope of the surface, σ the specific weight of sand, u_{*t} is the threshold saltation shear velocity using model constant A (0.1), z_m is the average saltation height and u_{st} is the minimum saltation velocity of grains in saltation.

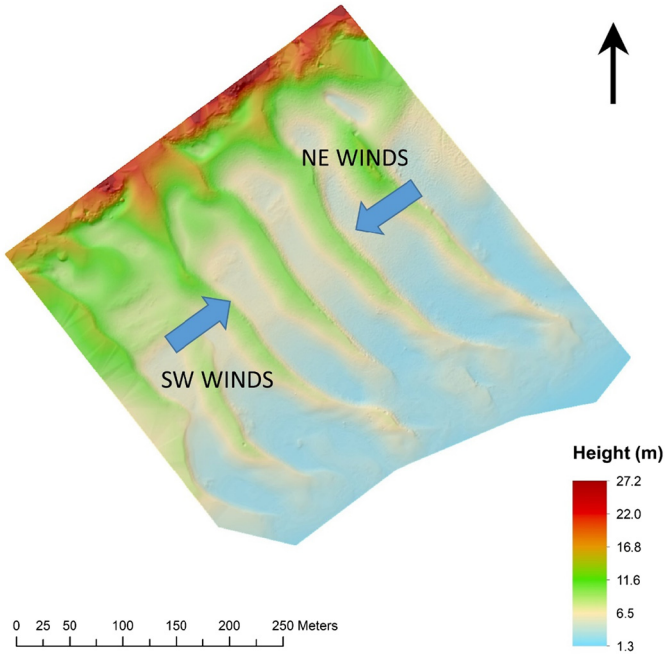

Fig. 3. The 3D Terrestrial Laser Scan surface generated showing the computational domain over which the CFD model was run. Modelled wind directions from the SW and NE were applied orthogonal to the dune crests.

3. Results

Several parameters extracted from the CFD simulations enabled a spatial examination of wind velocity, shear velocity as well as resulting aeolian flux over the multiple dune ridges under both wind direction scenarios.

3.1. Wind and shear velocities under SW directional winds

Under a SW wind direction, velocity streamlines show distinctive accelerated flow along all dune crests with maximum relative velocity ratios values ranging from 0.8 to 1.2. The relative velocity used here is the ratio of the local velocity (u) and the reference velocity at the inlet at 10 m of $u_{10} = 10$ ms^{-1}. This implies a wind speed near and above the dune crest of 8 to 12 ms^{-1} for the simulated wind speeds. Areas immediately in the lee of the crest streamlines were isolated to show complex lee-side interactions with the topography. For clarity reasons, Fig. 4A shows results of this only within the second and third ridges of the computational grid of dune topography. Results demonstrate a strong dominance of lee slope flow separation emerging off the crests whilst at the same time there is less turbulence on the stoss side of the dunes. Surface stress under this scenario also shows an even distribution across the upper part of the stoss area (Fig. 4B).

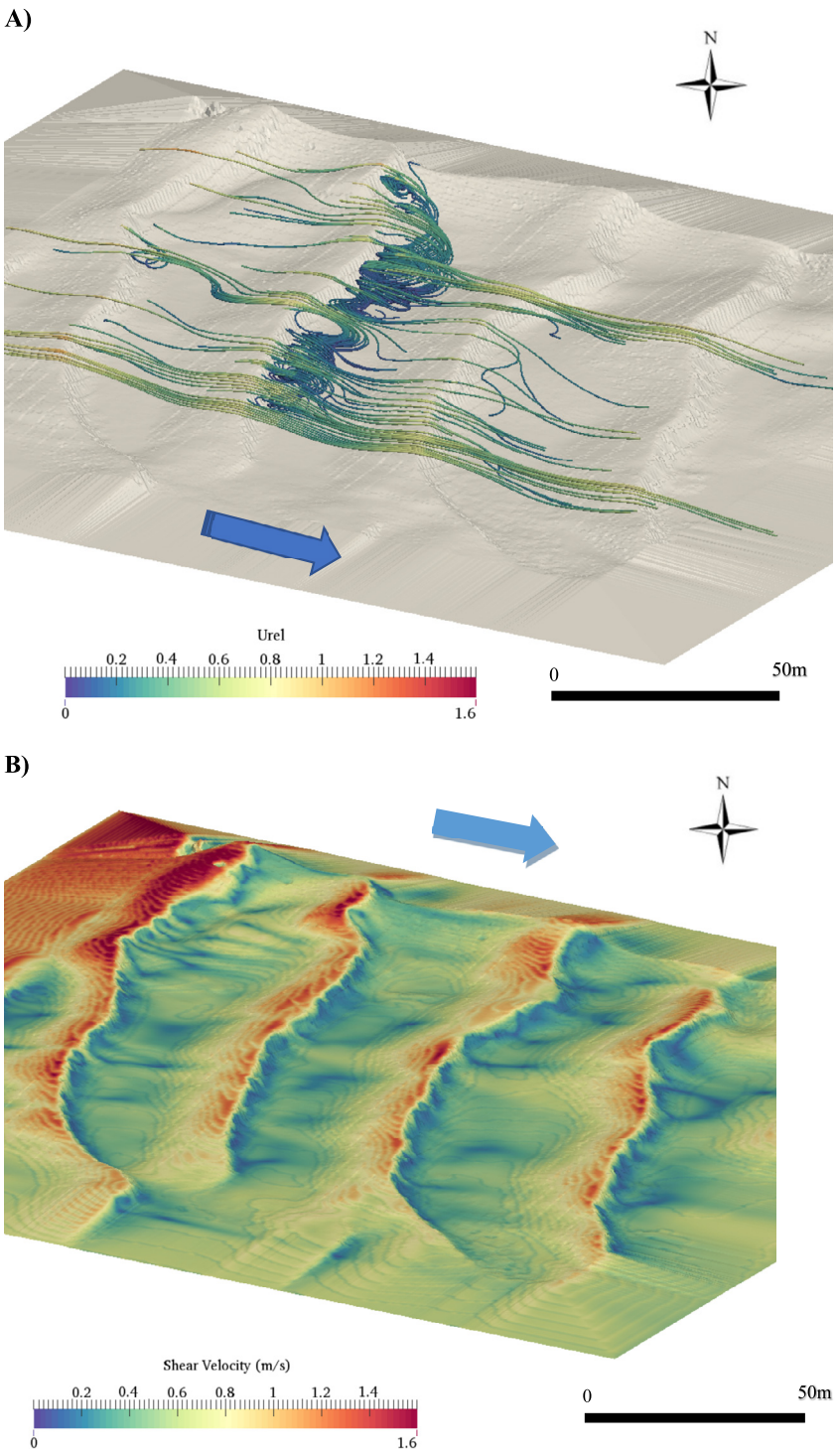

Fig. 4. A) Streamlines showing *detached* flow in lee and stronger *un-detached* flow above crests under SW flows. The colour scale is the ratio of the local near surface velocity and the inlet velocity at 10 m elevation (10 ms^{-1}). **B)** Surface shear velocity plot showing a more even distribution of stress across the stoss slopes under SW winds.

3.2. NE directional wind velocity simulations

A 180-degree flip in wind direction (from NE) simulating a reversal event, shows a distinct difference in flow behaviour across the dune surface compared to SW wind flows. Under a NE scenario (Fig. 5A), the topography of the dunes induces a significant reduction in flow separation behaviour, with the vast majority of flow remaining attached to the underlying surface. We also see surface shear stress concentrating more along the crests of the dunes (Fig. 5B), which can accelerate and focus the zone of potential aeolian transport within a smaller surface than with SW winds, suggesting a more restrictive zone of potential aeolian transport activation under less turbulent winds.

3.3. Differences in shear velocities between both directions

For clarity we label 'stoss' and 'lee' slopes as per topographical shape of the 3D surface being used for the CFD simulations i.e. stoss is the lower angle surface and lee is the steeper angle face of the dune. A direct comparison between SW and NE shear ve-

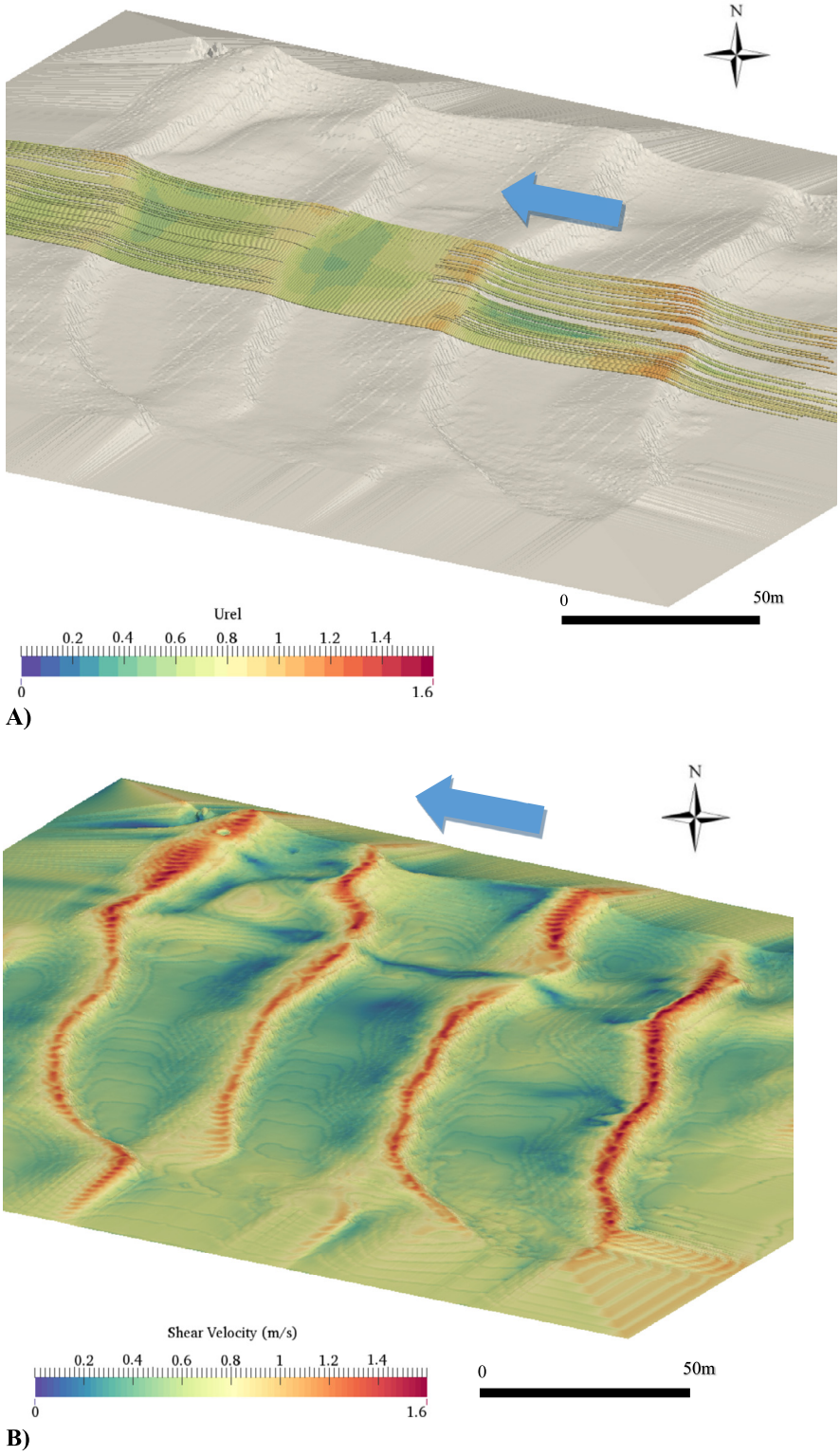

Fig. 5. A) Reversed wind direction (from NE) showing streamlines and largely *attached* flow in lee of dunes with now steeper inclined 'stoss' slopes focussing flow to the crests. The colour scale is the ratio of the local near surface velocity and the inlet velocity at 10 m elevation (10 ms^{-1}). **B)** Surface shear velocity plot showing a tightly focussed distribution of stress across the crest areas under NE winds.

locity simulations allows us to see where across the topography, larger differences are evident. When values are positive the SW shear velocity is dominant while negative values are showing NE shear velocity being dominant. This can infer where there is net transport in one direction over the other.

Immediately obvious is the larger (positive) differences (red) in shear velocity around the stoss slopes of the dunes under SW winds (Fig. 6). Much lower differences are on the slip face zones whereas shear velocity is much more dominant on the crestal edges under NE winds (negative values, blue).

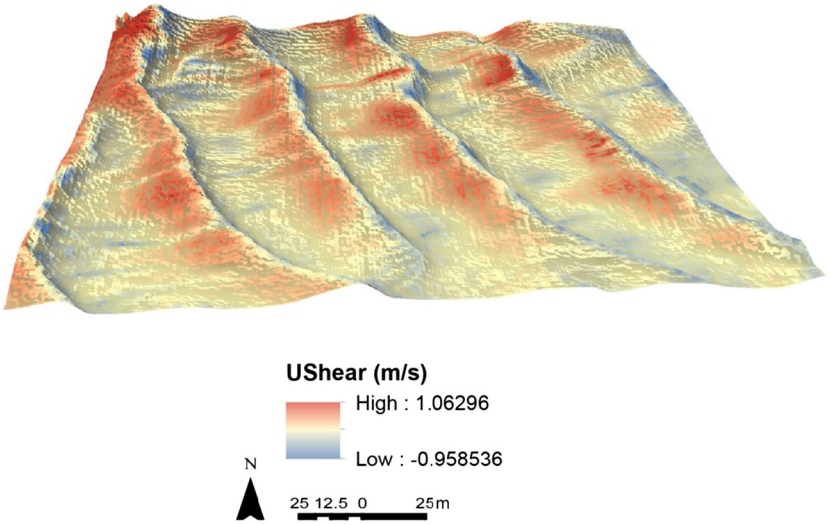

Fig. 6. Differences in shear velocities between SW and NE runs (i.e. SW minus NE at each grid point on the surface) showing larger differences.

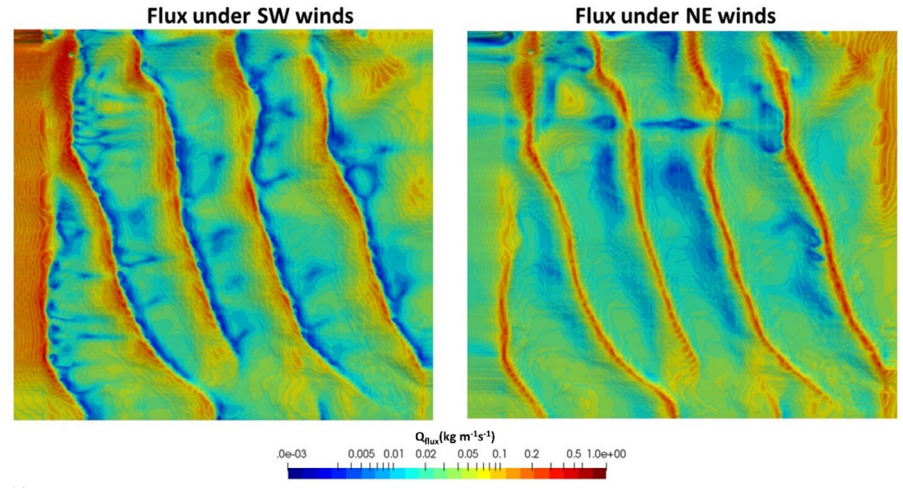

A)

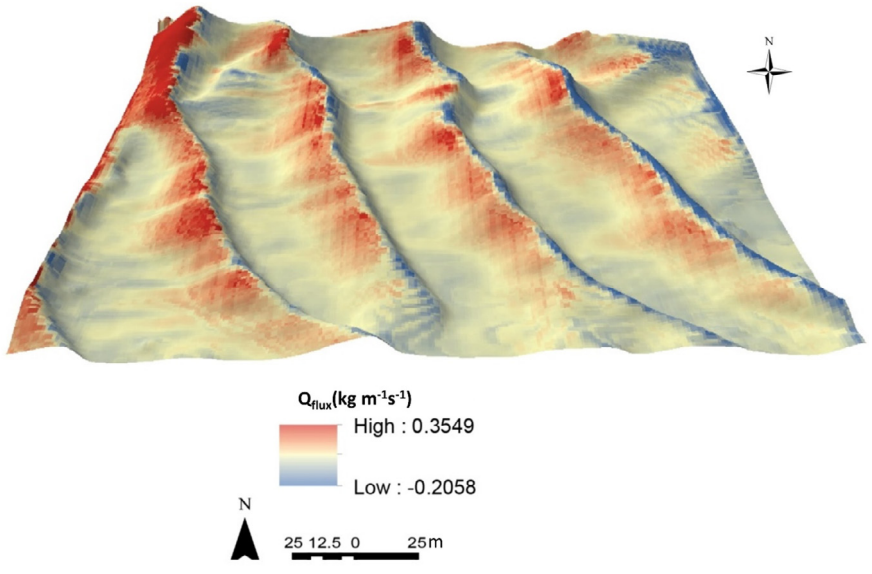

B)

Fig. 7. (A) Aeolian flux amounts, Q_{flux} ($kg\,m^{-1}\,s^{-1}$), produced (instantaneously) under each wind direction with SW winds (Left image) clustering on the stoss slopes while NE winds (Right Image) focus around the crest areas. **(B)** Difference map showing differential between SW minus NE airflow directions and resulting net Q_{flux}. Red represents positive and dominant SW flux whilst blue is more subordinate NE Q_{flux}.

3.4. Aeolian flux predictions

Wind-blown sediment potential flux under both directions over the dune surface are shown for both directions and total instantaneous flux amounts under both directions are calculated.

Following on from clear spatial differences in shear velocity under each direction, aeolian flux (Fig. 7A) which is directly associated with shear velocity, also displays distinctive spatial differences. SW winds manifest as higher flux on the stoss slopes, taking place over larger surface areas; whilst under NE winds, flux is concentrated more on the dune crest areas, over a smaller spatial area. Extracting SW and NE flux patterns from each other (SW minus NE) shows (Fig. 7B) positive or negative values of flux and the dominant direction of flux on the dune surfaces. Fig. 7B shows that in a direct comparison between both wind directions in a reversal situation, SW flows produce the dominant (positive, red) *net* flux over the dunes and this is focussed more on the dune stoss. A subordinate flux under NE flow also takes place and is focussed at and on the slip face side of the crest lines of the dune ridges.

Total instantaneous flux for SW winds over the total surface of the dunes was 1624 $kg\,m^{-1}\,s^{-1}$ whilst NE winds produced a total of 1487 $kg\,m^{-1}\,s^{-1}$ a reduction of around 10% and infers a net dune migration to the NE.

3.5. In situ observations of reversal events

When wind direction is reversed as modelled, on the ground observations show rapid (over several days) modification of dune morphology, particularly at the dune crests, where rounding and aerodynamically smoothing takes place (Fig. 8). Focussed surface winds under NE winds concentrate around the formerly sharp crested dune ridges and redistribute sediments down what were formerly stoss slopes.

Fig. 8. Ground level view of one of the reversing dune ridges at Mpekweni, South Africa at pre-reversal of wind flow (**Top**) with winds moving left to right and (**Bottom**) two days after reversal of winds where winds have smoothed the crests and winds are from right to left.

4. Discussion

Results show the behaviour of modelled wind flow over transverse dunes under opposing (reversing) wind directions. During SW winds that traverse typical dune form topography (incident long stoss slope, short slipface dimensions), flow behaves in a classic fashion where detachment and stoss side shear stress is evenly spread over gentle slopes with large undulating low shear zones in leeward wake of crests. Streamlines show clear evidence of 3D flow, helical flow separation detachment and effectively a reverse eddy return flow back up the dune slip face. Q_{flux} associated with SW winds is the dominant overall flux present with most transport being generated under these winds. The stoss slopes are the primary area activated under these winds and are where the majority of the sand transport is found, helping to drive dune migration to a NE direction. Field observations show that these SW flow scenarios effectively maintain the downwind sediment transport pathway (and dune shape) with energy spread evenly across the stoss face, feeding the brink and slipface with sediment and helping migrate the dune forward, maintaining the transverse dune form. Under SW winds significant flow steering and re-direction takes place as the SW flow has distinct flow separation. SW flows also show (compared to NE flow scenario) typically increased u_* on the stoss slope (but distributed over a larger area) and contains large, undulating low shear zones in the leeward wakes (slip face and interdune zones).

When flow is reversed (NE winds), model results show that stress is initially more focussed along the crests than the upper stoss area, which likely produces higher vertical disturbance into the boundary layer with the change in aerodynamics of the flow. Former slip-faces now face into the incident winds, focussing airflow energy over smaller areas, thereby raising potential aeolian transport and rounding action of the once sharp-edged dune brink zone. Simulated flow separation and steering for the reversed NE wind is heavily suppressed, likely due to the steep change in the new 'stoss' slope. Q_{flux} in NE wind scenarios again shows most sand transport occurring at and slightly below (on the slip face) the dune crests. Overall, if winds are reversed and the topography is as it was surveyed, then the impact under SW winds will be more pronounced and flux dominance prevails with approximately 10% more transport occurring under SW flows compared to NE flows. This airflow reversal therefore helps drive the reversing topographical phenomena at the site, with NE winds initially focussing round the crests and then migrating dunes to the SW. The study provides new insights into dune migration behaviour as well as surface flow behaviour across multiple dune configurations and length scales within un-vegetated dune fields and play a crucial role in overall dune field dynamics. Results highlight the complex nature of reversing transverse dunes, where it is likely that with the onset of flow reversal, dunes may initially round their formerly sharp crests (see Fig. 8 field observation) and with focussed shear stress, then eventually reform into transverse dunes in the opposite direction.

The work also demonstrates the applicability of CFD analysis of simple-to-sinuous transverse aeolian bedforms with ~50 m wavelength and ridge heights of a few metres. Landforms of a very similar scale and morphology are also found on Mars (Fig. 9): "Transverse Aeolian Ridges" or TARs (e.g. Balme et al., 2008; Fig. 12). TARs are thought to form as megaripples, rather than as reversing dunes, based on analysis of their cross sectional profiles and

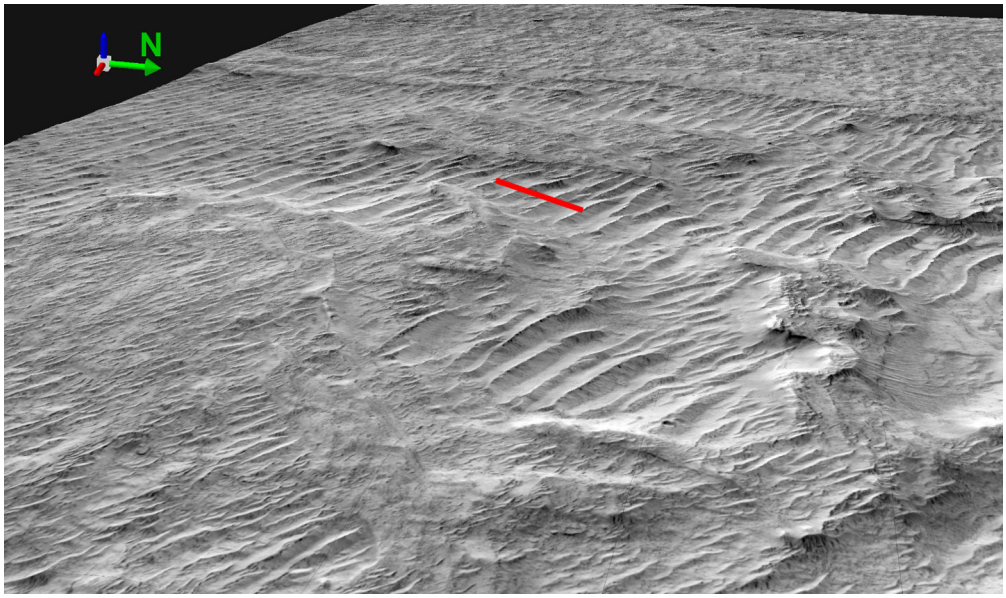

Fig. 9. Transverse Aeolian Ridges on Mars. Red bar is 250 m long. Note these simple transverse bedforms are of similar scale to the Mpekweni dunes, having down-wind lengths of 50-60 m and heights of 3-5 m. Part of HiRISE (McEwen et al., 2007) image number ESP_021577_1920 overlain on a Digital Elevation model created using stereo photogrammetry from this image and number ESP_022434_1920. There is no vertical exaggeration; lighting is from the top of the image. Digital Elevation Model created by Joel Davis and Peter Grindrod at Natural History Museum UK. Original image data credit NASA/JPL/UoA.

morphometric similarity to megaripples on Earth (e.g. Hugenholtz et al., 2017), and observations by Mars rovers of coarse (granule grade) particles mantling large ripples (e.g. Sullivan et al., 2005). Moreover, TARs are generally thought to be immobile on Mars, whereas shape changes and ripple-migration on large Martian dunes demonstrates that these features are actively migrating (e.g. Bourke et al., 2008; Silvestro et al., 2010). CFD studies of TARs could help answer the ongoing question of why these metre-scale bedforms almost always appear immobile, whereas many hundred metre-scale martian duneforms are clearly migrating (Bourke et al., 2008; Silvestro et al., 2010). CFD can do this by characterising the aerodynamic shear stress these bedforms are subjected to, and hence determining what flux of fine-grained sand they experience. In combination with Mars climate models, these results could then help determine the mechanisms and climate epochs under which the TARs formed, and why these are less mobile than their larger duneform cousins.

5. Conclusions

The study modelled airflow behaviour over transverse (reversing) dune ridges at the onset of airflow reversal. Using fine (submetre scale) CFD modelling, 3D airflow patterns were quantified across multiple dune ridges and spatial patterns of shear stress and associated Q_{flux} were evaluated. SW flows over typical transverse dune profiles produced the dominant flux conditions, which focussed largely on the stoss slopes, while NE flows focussed transport along the dune crests and over smaller areas. The CFD work presented here provides important analogue information to study similar bedform features on Mars, and helps give detailed insights into what airflow characteristics may have been required to migrate such dune features in the past or present.

Author contributions

Derek Jackson performed writing (original draft and conceptualization), fieldwork, analysis of CFD output and interpretation. Andrew Cooper and Andrew Green performed fieldwork and reviewing of text; Meiring Beyers performed CFD computation analysis and method writing; Emilia Guisado-Pintado performed review and editing, analysis and display of CFD output; Errol Wiles and Keegan Benallack performed fieldwork; Matt Balme contributed to the editing and reviewing of the manuscript.

Declaration of competing interest

The authors declare that they have no known competing financial interests or personal relationships that could have appeared to influence the work reported in this paper.

Acknowledgements

Funding: This work is a contribution to the Natural Environment Research Council grant NE/F019483/1. We thank Dave Rogers, Ulster University for assisting with merging of the TLS data sets.

References

Anderson, W., Chamecki, M., 2014. Numerical study of turbulent flow over complex aeolian dune fields: the White Sands National Monument. Phys. Rev. E 89 (1), 013005. https://doi.org/10.1103/PhysRevE.89.013005.

Bagnold, R.A., 1941. The Physics of Blown Sand and Desert Dunes. Methuen, London.

Balme, M., Berman, D.C., Bourke, M.C., Zimbelman, J.R., 2008. Transverse Aeolian Ridges (TARs) on Mars. Geomorphology 101 (4), 703–720. https://doi.org/10.1016/j.geomorph.2008.03.011.

Bourke, M.C., Edgett, K.S., Cantor, B.A., 2008. Recent aeolian dune change on Mars. Geomorphology 94 (1), 247–255. https://doi.org/10.1016/j.geomorph.2007.05.012.

Bristow, C.S., Augustinus, P.C., Wallis, I.C., Jol, H.M., Rhodes, E.J., 2010. Investigation of the age and migration of reversing dunes in Antarctica using GPR and OSL, with implications for GPR on Mars. Earth Planet. Sci. Lett. 289 (1), 30–42. https://doi.org/10.1016/j.epsl.2009.10.026.

Bristow, N.R., Blois, G., Best, J.L., Christensen, K.T., 2019. Spatial scales of turbulent flow structures associated with interacting barchan dunes. J. Geophys. Res., Earth Surf. 124 (5), 1175–1200. https://doi.org/10.1029/2018jf004981.

Burkinshaw, J.R., Rust, I.C., 1993. Aeolian dynamics on the windward slope of a reversing transverse dune, Alexandria coastal dunefield, South Africa. In: Aeolian Sediments, pp. 13–21.

Burkinshaw, J.R., Illenberger, W.K., Rust, I.C., 1993. Wind-speed profiles over a reversing transverse dune. Geol. Soc. (Lond.) Spec. Publ. 72 (1), 25–36. https://doi.org/10.1144/gsl.sp.1993.072.01.04.

Chojnacki, M., Burr, D.M., Moersch, J.E., Michaels, T.I., 2011. Orbital observations of contemporary dune activity in Endeavor crater, Meridiani Planum, Mars. J. Geophys. Res., Planets 116 (E7). https://doi.org/10.1029/2010je003675.

Cooper, J.A.G., Smith, A.M., Green, A.N., 2013. Backbeach deflation aprons: morphology and sedimentology. J. Sediment. Res. 83, 395–405. https://doi.org/10.2110/jsr.2013.34.

Cornish, V., 1897. On the formation of sand dunes. Geogr. J. 9, 278–302.

Cornwall, C., Jackson, D.W.T., Bourke, M.C., Beyers, M., Cooper, J.A.G., 2018. Seasonal variations in airflow over the Namib dune, Gale Crater, Mars: implications for dune dynamics. Geophys. Res. Lett. 45 (18), 9498–9507. https://doi.org/10.1029/2018GL079598.

Courrech du Pont, S., Narteau, C., Gao, X., 2014. Two modes for dune orientation. Geology 42 (9), 743–746. https://doi.org/10.1130/g35657.1.

Dann, J., 1939. Sandgebirge in Alagschan (sand hills in Alagschan). Z. Geomorphol. 11 (1), 28–51.

Gao, X., Narteau, C., Rozier, O., Courrech du Pont, S., 2015. Phase diagrams of dune shape and orientation depending on sand availability. Sci. Rep. 5, 14677. https://doi.org/10.1038/srep14677.

Greeley, R., Iversen, J.D., 1985. Wind as a Geological Process on Earth, Mars, Venus and Titan, 05/01 ed. Cambridge University Press, Cambridge, London, New York, New Rochelle, Melbourne, Sydney, 333 pp.

Haberle, R.M., Pollack, J.B., Barnes, J.R., Zurek, R.W., Leovy, C.B., Murphy, J.R., Lee, H., Schaeffer, J., 1993. Mars atmospheric dynamics as simulated by the NASA Ames General Circulation Model: 1. The zonal-mean circulation. J. Geophys. Res., Planets 98 (E2), 3093–3123. https://doi.org/10.1029/92je02946.

Hugenholtz, C.H., Barchyn, T.E., Boulding, A., 2017. Morphology of transverse aeolian ridges (TARs) on Mars from a large sample: further evidence of a megaripple origin? Icarus 286, 193–201. https://doi.org/10.1016/j.icarus.2016.10.015.

Illenberg, W.K., Rust, I.C., 1988. A sand budget for the Alexandria coastal dunefield, South Africa. Sedimentology 35 (3), 513–521. https://doi.org/10.1111/j.1365-3091.1988.tb01001.x.

Jackson, D.W.T., Beyers, J.H.M., Lynch, K., Cooper, J.A.G., Baas, A.C.W., Delgado-Fernandez, I., 2011. Investigation of three-dimensional wind flow behaviour over coastal dune morphology under offshore winds using computational fluid dynamics (CFD) and ultrasonic anemometry. Earth Surf. Process. Landf. 36 (8), 1113–1124. https://doi.org/10.1002/esp.2139.

Jackson, D.W.T., Beyers, J.H.M., Delgado-Fernandez, I., Baas, A.C.W., Cooper, J.A.G., Lynch, K., 2013a. Airflow reversal and alternating corkscrew vortices in foredune wake zones during perpendicular and oblique offshore winds. Geomorphology 187, 86–93. https://doi.org/10.1016/j.geomorph.2012.12.037.

Jackson, D.W.T., Cruz-Avero, N., Smyth, T.A.G., Hernández-Calvento, L., 2013b. 3D airflow modelling and dune migration patterns in an arid coastal dune field. J. Coast. Res. SI 65, 1301–1306. https://doi.org/10.2112/SI65-220.1.

Jackson, D.W.T., Bourke, M.C., Smyth, T.A.G., 2015. The dune effect on sand-transporting winds on Mars. Nat. Commun. 6, 8796. https://doi.org/10.1038/ncomms9796.

King, W.H.J., 1918. Study of a dune belt. Geogr. J. 47, 189–209.

Lewis, S.R., Collins, M., Read, P.L., Forget, F., Hourdin, F., Fournier, R., Hourdin, C., Talagrand, O., Huot, J.-P., 1999. A climate database for Mars. J. Geophys. Res., Planets 104 (E10), 24177–24194. https://doi.org/10.1029/1999je001024.

Lindsay, J.F., 1973. Reversing barchan dunes in lower Victoria Valley, Antarctica. GSA Bull. 84 (5), 1799–1806. https://doi.org/10.1130/0016-7606(1973)84.

McEwen, A.S., Eliason, E.M., Bergstrom, J.W., Bridges, N.T., Hansen, C.J., Delamere, W.A., Grant, J.A., Gulick, V.C., Herkenhoff, K.E., Keszthelyi, L., Kirk, R.L., Mellon, M.T., Squyres, S.W., Thomas, N., Weitz, C.M., 2007. Mars reconnaissance orbiter's high resolution imaging science experiment (HiRISE). J. Geophys. Res., Planets 112 (E5). https://doi.org/10.1029/2005je002605.

McKee, E.D., 1979. A study of global sand seas. Report Rep., 439 pp., Washington, DC.

Paterson, D.A., Holmes, J.D., 1993. Computation of wind flow over topography. J. Wind Eng. Ind. Aerodyn. 46–47, 471–476. https://doi.org/10.1016/0167-6105(93)90314-E.

Richards, P.J., Hoxey, R.P., 1993. Appropriate boundary conditions for computational wind engineering models using the k-ϵ turbulence model. J. Wind Eng. Ind. Aerodyn. 46–47, 145–153. https://doi.org/10.1016/0167-6105(93)90124-7.

Selby, M.J., Rains, R.B., Palmer, R.W.P., 1974. Eolian deposits of the ice-free Victoria Valley, southern Victoria Land, Antarctica. N.Z. J. Geol. Geophys. 17 (3), 543–562. https://doi.org/10.1080/00288306.1973.10421580.

Silvestro, S., Fenton, L.K., Vaz, D.A., Bridges, N.T., Ori, G.G., 2010. Ripple migration and dune activity on Mars: evidence for dynamic wind processes. Geophys. Res. Lett. 37 (20). https://doi.org/10.1029/2010gl044743.

Silvestro, S., Vaz, D.A., Ewing, R.C., Rossi, A.P., Fenton, L.K., Michaels, T.I., Flahaut, J., Geissler, P.E., 2013. Pervasive aeolian activity along rover Curiosity's traverse in Gale Crater, Mars. Geology 41 (4), 483–486. https://doi.org/10.1130/g34162.1.

Smith, A.B., Jackson, D.W.T., Cooper, J.A.G., 2017a. Three-dimensional airflow and sediment transport patterns over barchan dunes. Geomorphology 278, 28–42. https://doi.org/10.1016/j.geomorph.2016.10.025.

Smith, A.B., Jackson, D.W.T., Cooper, J.A.G., Hernández-Calvento, L., 2017b. Quantifying the role of urbanization on airflow perturbations and dunefield evolution. Earth's Future 5 (5), 520–539. https://doi.org/10.1002/2016EF000524.

Smyth, T.A.G., 2016. A review of computational fluid dynamics (CFD) airflow modelling over aeolian landforms. Aeolian Res. 22, 153–164. https://doi.org/10.1016/j.aeolia.2016.07.003.

Smyth, T.A.G., Jackson, D.W.T., Cooper, J.A.G., 2011. Computational Fluid Dynamic Modelling of Three-Dimensional Airflow over Dune Blowouts, pp. 314–318.

Smyth, T.A.G., Jackson, D.W.T., Cooper, J.A.G., 2012. High resolution measured and modelled three-dimensional airflow over a coastal bowl blowout. Geomorphology 177–178, 62–73. https://doi.org/10.1016/j.geomorph.2012.07.014.

Smyth, T.A.G., Jackson, D.W.T., Cooper, J.A.G., 2013. Three dimensional airflow patterns within a coastal trough–bowl blowout during fresh breeze to hurricane force winds. Aeolian Res. 9, 111–123. https://doi.org/10.1016/j.aeolia.2013.03.002.

Smyth, T.A.G., Jackson, D., Cooper, A., 2014. Airflow and aeolian sediment transport patterns within a coastal trough blowout during lateral wind conditions. Earth Surf. Process. Landf. 39 (14), 1847–1854. https://doi.org/10.1002/esp.3572.

Spiga, A., Forget, F., 2009. A new model to simulate the Martian mesoscale and microscale atmospheric circulation: validation and first results. J. Geophys. Res., Planets 114 (E2). https://doi.org/10.1029/2008je003242.

Sullivan, R., Banfield, D., Bell, J.F., Calvin, W., Fike, D., Golombek, M., Greeley, R., Grotzinger, J., Herkenhoff, K., Jerolmack, D., Malin, M., Ming, D., Soderblom, L.A., Squyres, S.W., Thompson, S., Watters, W.A., Weitz, C.M., Yen, A., 2005. Aeolian processes at the Mars Exploration Rover Meridiani Planum landing site. Nature 436 (7047), 58–61. https://doi.org/10.1038/nature03641.

Sullivan, R., Arvidson, R., Bell III, J.F., Gellert, R., Golombek, M., Greeley, R., Herkenhoff, K., Johnson, J., Thompson, S., Whelley, P., Wray, J., 2008. Wind-driven particle mobility on Mars: insights from Mars Exploration Rover observations at "El Dorado" and surroundings at Gusev Crater. J. Geophys. Res., Planets 113 (E6). https://doi.org/10.1029/2008je003101.

Tinley, K.L., 1985. Coastal dunes of South Africa. South African National Scientific Programs Report Rep. 109, 1-297 pp.

Toigo, A.D., Richardson, M.I., 2002. A mesoscale model for the martian atmosphere. J. Geophys. Res., Planets 107 (E7), 3-1–3-21. https://doi.org/10.1029/2000je001489.